Probing protein structure and dynamics by second-derivative ultraviolet absorption analysis of cation–π interactions

LAURA H. LUCAS,[1,2] BARAN A. ERSOY,[1,3] LISA A. KUELTZO,[4] SANGEETA B. JOSHI, DUANE T. BRANDAU, NAGARAJAN THYAGARAJAPURAM, LAURA J. PEEK, AND C. RUSSELL MIDDAUGH

Department of Pharmaceutical Chemistry, University of Kansas, Lawrence, Kansas 66047, USA

(RECEIVED February 2, 2006; FINAL REVISION June 22, 2006; ACCEPTED July 7, 2006)

Abstract

We describe an alternate approach for studying protein structure using the detection of ultraviolet (UV) absorbance peak shifts of aromatic amino acid side chains induced by the presence of salts. The method is based on the hypothesis that salt cations (Li^+, Na^+, and Cs^+) of varying sizes can differentially diffuse through protein matrices and interact with benzyl, phenyl, and indole groups through cation–π interactions. We have investigated the potential of this method to probe protein dynamics by measuring high resolution second-derivative UV spectra as a function of salt concentration for eight proteins of varying physical and chemical properties and the *N*-acetylated *C*-ethyl esterified amino acids to represent totally exposed side chains. We show that small shifts in the wavelength maxima for Phe, Tyr, and Trp in the presence of high salt concentrations can be reliably measured and that the magnitude and direction of the peak shifts are influenced by several factors, including protein size, charge, and the local environment and solvent accessibility of the aromatic groups. Evaluating the empirical UV spectral data in light of known protein structural information shows that probing cation–π interactions in proteins reveals unique information about the influence of structure on aromatic side chain spectroscopic behavior.

Keywords: cation–π interactions; second derivative UV spectra; protein structure; dynamics; peak shift; aromatic amino acids; side chains

Supplemental material: see www.proteinscience.org.

Dynamic aspects of protein structure have become of increasing interest due to their potential role in protein structure, stability, and function. The structure and motions of polypeptide chains in proteins can be studied by a number of methods, each yielding a different picture of the dynamic structure due to the time scale and magnitude of the motions that can be probed by a particular technique. High resolution pictures are achievable using NMR (Keniry and Carver 2002; Adams et al. 2004), ESR (Poluektov et al. 2003), crystallographic temperature factors (Yuan et al. 2003), isotope exchange monitored by mass spectrometry (Zhang and Smith 1993; Yan et al. 2004) and infrared spectroscopy (Yu et al. 2004). A somewhat lower resolution but unique picture of protein dynamic behavior is provided by using small neutral solutes such as O_2 and acrylamide (Lakowicz et al. 1983; Fasano et al. 2003; Ruiz et al. 2003) to study

[1]These authors contributed equally to this work.

Present addresses: [2]Procter and Gamble, 5289 Vine St., #1303, Cincinnati, OH 45217, USA; [3]Department of Biopharmaceutical Sciences, University of California, San Francisco, CA 94143, USA; [4]University of Colorado Health Sciences Center, Department of Pharmaceutical Sciences, Denver, CO 80262, USA.

Reprint requests to: C. Russell Middaugh, Department of Pharmaceutical Chemistry, University of Kansas, 2030 Becker Drive, Lawrence, KS 66047, USA; e-mail: middaugh@ku.edu; fax: (785) 864-5814.

Article published online ahead of print. Article and publication date are at http://www.proteinscience.org/cgi/doi/10.1110/ps.062133706.

the quenching of intrinsic protein fluorescence. In this approach, the diffusion of solutes through protein matrices is thought to be limited by local internal structural motions that control the collision rate between quenchers and target fluorophores. In most cases, these fluorophores are limited to the indole side chain of tryptophan, a relatively scarce amino acid. This can be advantageous since the site of the quenching reaction can be well defined by the presence of a single Trp residue, but also limits the possibility of observing more global effects on protein dynamics.

To obtain a more complete picture of protein structure and dynamics, ultraviolet absorbance spectroscopy can be used to monitor signals from the three aromatic amino acids: Phe, Tyr, and Trp. The absorbance spectra of these amino acids each contain several broad overlapping peaks between 200 and 300 nm, the weaker of which do not overlap with the absorbance bands of peptide bonds. These weaker bands arise from π-π* transitions involving electrons of the aromatic rings (Donovan 1969; Wetzel et al. 1980). Calculating the derivative of an absorbance curve enhances resolution and facilitates deconvolution of complex zero order spectra (Giese and French 1955; Grum et al. 1972). In the second derivative of the spectrum ($d^2A/d\lambda^2$), the absorbance arising from these residues is resolved as minima in the spectral regions 245–270 nm (Phe), 265–285 (Tyr), and 265–295 nm (Trp), and thus spectral overlap is significantly reduced (Ichikawa and Terada 1977; Balestrieri et al. 1978; Levine and Federici 1982; Kueltzo et al. 2003).

Recent developments in high resolution ultraviolet absorbance spectroscopy permit the position of derivative peaks to be defined to a resolution approaching 0.01 nm. This ability arises from the very high precision of modern diode array spectrometers. Although the intrinsic resolution of such instruments is typically only 1.0–2.0 nm due to diode spacing, interpolation of this data permits a much higher effective resolution to be obtained (Mach et al. 1991). Thus, quite small shifts in peak positions can be detected and are the basis for the studies described here. Analysis of second-derivative UV spectra has been used to quantitate amino acid content (Ichikawa and Terada 1977, 1979; Balestrieri et al. 1978, 1980; Levine and Federici 1982), detect conformational changes in terms of alterations in aromatic side chain microenvironments (Solli and Herskovits 1973; Ichikawa and Terada 1979; Mach et al. 1991; Mach and Middaugh 1994), and, more recently, to generate empirical phase diagrams to analyze protein stability over a range of solution conditions (Kueltzo et al. 2003). To complement these existing applications, the method described herein uses cations and their interactions with the π electrons of the aromatic groups of Phe, Tyr, and Trp to attempt to probe the features of protein structure influencing such interactions.

Cation–π interactions can be qualitatively described by an electrostatic model, although dispersion forces and polarizability also influence these effects (Dougherty 1996; Ma and Dougherty 1997). Much of the electron density in an aromatic ring is actually delocalized in the π orbitals above and below the plane of the ring, creating a molecular quadrupole that can attract cations. Theoretical studies have shown that the aromatic amino acids Phe, Tyr, and Trp have significant quadrupole moments (Bohórquez et al. 2003) and interact with cations (Ryzhov et al. 2000; Rogers and Hirst 2003; Ruan and Rodgers 2004). Soluble proteins are generally folded such that the apolar amino acids are, on average, buried in the interior, away from the solvent-exposed surface. In general, Phe residues tend to be completely buried in protein interiors due to the apolarity of the benzene ring, while the Trp and Tyr side chains of indole and phenol are often differentially distributed from the interior to the surface due to the presence of electronegative nitrogen and oxygen atoms, respectively, in their structures. While it is well established that cations can pair with negatively charged, surface-exposed residues such as aspartate and glutamate, it is also well known that more basic side chains (Lys, Arg, His) can form cation–π interactions with aromatic side chains and may be involved in enzyme catalysis (Dougherty 1996; Ma and Dougherty 1997), ion transport through cell membranes (Dougherty 1996; Ma and Dougherty 1997), and protein–protein interactions (Woods 2004).

The approach we describe is based on using high salt concentrations to drive the diffusion of cations into interior regions of proteins such that the cations interact with the aromatic amino acid side chains. The chloride salts of three cations (Li^+, Na^+, and Cs^+) were chosen on the basis of their varying size (Table 1). By comparing the ability of the three cations to shift the positions of aromatic absorbance peaks, we should be able to obtain information about the local structure and dynamics of the protein matrix that permit the cations to form cation–π contacts. We initially establish the basis of the technique using uncharged model aromatic amino acids and then investigate a series of proteins with varying degrees of

Table 1. *Sizes and enthalpies of hydration of monovalent cations used as protein structural probes*

Cation	Li^+	Na^+	Cs^+
Unhydrated radius (Å)[a]	0.76	1.02	1.74
Hydrated radius (Å)[b]	6.0	4.5	2.5
$\Delta H_{hydration}$ (kJ/mol)[c]	−549	−440	−298

[a] Ionic radii reported by Shannon (1976), based on appropriate coordination geometry with Cl^-.
[b] Rounded values given by Kielland (1937).
[c] As reported by Edsall and McKenzie (1978).

exposure of particular side chains. These studies establish that this approach can detect significant differences in the interactions of the aromatic residues of different proteins with cations due to unique structural features that influence the dynamic behavior of proteins in the presence of high salt concentrations.

Results

Interactions of cations with the model aromatic amino acid side chains

Figure 1 shows the relative peak shifts for *N*-acetylated carboxyl ethyl esters of Phe, Trp, and Tyr as a function of cation type and concentration. Amino acids *N*-acetylated and esterified at the C termini were chosen to minimize electrostatic interactions that could complicate interpretation of spectral changes due to cation–π effects between the salts and the aromatic rings of the amino acids. Although several peaks are observed in the second-derivative UV spectra for each amino acid (Supplemental Figs. S1–S3), one peak was selected for comparison with the data obtained for several different proteins. The peaks selected for each amino acid display no significant overlap. Noncovalent interactions between the cations and the aromatic side chains appear to be relatively weak, since most of the changes in peak position fail to saturate at even the highest salt concentrations tested. This is complicated, however, by potential changes in peak position induced by alterations in dielectric constant. A plateau is observed for Cs^+ in the Phe peaks (Fig. 1A), but this only occurred at very high salt concentration and represented a relatively small change in the overall peak position. All three cations do not induce large differential peak shifts until 1.5 M salt concentration, but the shifts seen at lower salt concentration are highly reproducible. High salt concentrations shift the second derivative UV peaks for Phe and Trp (Fig. 1B) to longer wavelengths (red shifts). These results are consistent with those observed by Padrós et al. (1982) when Phe is exposed to solvents of increasing apolarity. Since Phe and Trp in these studies are in an aqueous environment, the results in Figure 1A,B may indicate that cations somewhat shield the ring from water and that, as expected, high salt concentrations facilitate the cation–π interactions with Trp. To insure that the observed effects were due to cation–π interactions and not direct association of the ions with the amide and carboxyl side groups, titrations were also performed with 1-amino toluene (phenylalanine analog), serotonin (tryptophan analog), and 4-methyl phenol (tyrosine analog). This data (Supplemental Fig. S4) shows similar shifts in peak position as seen with the model amino acids supporting the presence of cation–π interaction. 3-Methylindole was not used as a tryptophan analog due to its limited solubility.

The cations seem to induce much more dramatic peak shifts in the Tyr spectra (Fig. 1C). Cesium causes a large red (positive) shift, Na^+ a small blue (negative) shift, while Li^+ causes a large negative change, approximately equal in magnitude to the red shift effected by Cs^+. The differences in these shifts are also clear at much lower concentrations (~0.25 M), suggesting that Tyr peak position is more sensitive to both cation size or charge density and concentration than Phe or Trp. Ito (1960) has reported that wavelength shifts in the absorbance bands of phenol reflect hydrogen bond formation, with red shifts observed when phenol acts as a proton donor and blue shifts seen when it serves as a proton acceptor. Increased ionic strength also favors dissociation of Tyr (Harris 1995), shifting the equilibrium to the deprotonated phenolate anion that could act as a proton acceptor. High concentrations of Li^+ and Na^+ thus cause a blue shift consistent with phenolate hydrogen bonding to the solvent or the hydrated cations themselves.

A red shift is observed when Cs^+ is used, suggesting that the phenol group of Tyr may be acting as a proton donor. The extent of Tyr deprotonaton should be the same

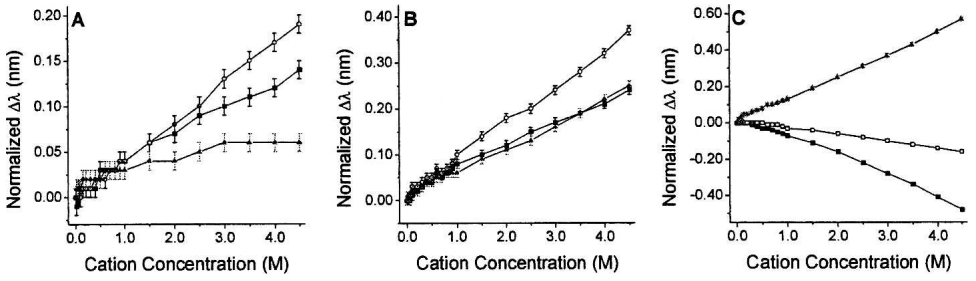

Figure 1. Peak shifts (Δλ) in the second-derivative UV absorption spectra for the model amino acids *N*-acetyl-L-phenylalanine ethyl ester (*A*), *N*-acetyl-L-tryptophan ethyl ester (*B*), and *N*-acetyl-L-tyrosine ethyl ester (*C*) induced by the cations Li^+ (■), Na^+ (○), and Cs^+ (▲). The peak positions at each concentration point are normalized by subtracting the initial peak positions, which were 257.94 ± 0.01 nm (Phe), 289.32 ± 0.01 nm (Trp), and 275.01 ± 0.01 nm (Tyr). Error bars represent the standard deviation of the mean for $n = 3$ for each salt. If the error bars are not seen, they are subsumed with the data point.

when Li^+ or Na^+ is used, however, since the change in ionic strength is identical. The hydroxyl group of Tyr is a known auxochrome, which does not absorb in the near UV region but influences the positions of the aromatic absorbance peaks (Skoog et al. 1998). The nonbonding electrons of oxygen can interact with the π ring electrons and stabilize the π* electronic energy state, thus effecting a red shift (Skoog et al. 1998). Generally, the auxochromic effect is greater for phenolate than phenol due to the additional pair of nonbonding electrons on oxygen (Skoog et al. 1998). In examining the results presented here, note that the Cs^+ possesses a much smaller hydration shell and $\Delta H_{hydration}$ than Li^+ and Na^+ (Table 1). This suggests that the hydrogen bonding effects described above are much less likely to occur, resulting in domination of the underlying auxochromic effect and the observed red shift in the Tyr peak position.

Interactions of cations with aromatic amino acid side chains in proteins

Proteins displaying a variety of sizes, secondary structure, and isoelectric points were selected to investigate the ability of cations to interact with protein aromatic residues. Table 2 lists some physical and chemical properties for the monomeric units of these proteins. Several single Trp-containing proteins were examined, thus at least in principle permitting effects on single residues to be resolved. Crystallographic data, however, suggest that many of these proteins self-associate to form multimeric structures. Thus, our results reflect a weighted average of the cations interacting with an equilibrium mixture of each protein in its various forms.

Generally, the Phe peak shifts for the proteins studied were relatively small, although clearly present. Noise was sufficient that it was difficult to discern clear trends in the data with respect to cation size (Fig. 2). This is probably an immediate consequence of the relatively low extinction coefficient of Phe compared to Trp and Tyr and the fact that these residues are generally more buried within the protein matrix where it would be more difficult for the charged cations to penetrate. The proteins KGF-2 and L-asparaginase (Fig. 2A and F, respectively) show more pronounced shifts, but there does not seem to be a common physical or chemical feature between these proteins (Table 2) that would explain the greater shifts. The results in Figure 2 do suggest that the Phe groups in these proteins are more accessible to cations than those in the other proteins examined.

To assist in the analysis of these empirical spectral data, solvent accessible surface areas were calculated for the aromatic amino acids using available crystal structures for the proteins studied (Table 3). The values in Table 3 can be compared to each other to determine relative exposures of the different types of aromatic amino acids, in the absence of salt. Although these values do not directly indicate the accessibility of aromatic groups to cations, a higher degree of solvent accessibility suggests an increased likelihood that the aromatic groups would also be accessible to cations. Since the model amino acids yielded solvent accessible surface areas >200 Å, the data in Table 3 reflect an influence of neighboring residues on physically restricting cation–π interactions, even if the aromatic groups are positioned on the protein surface. The observation that the Phe peak shifts are most pronounced for KGF-2 and L-asparaginase may also be

Table 2. *Physical and chemical properties of proteins studied*

Protein[a] (dominant secondary structure element)[b]	No. subunits[c]	Residues per subunit	Subunit MW (kDa)	No. Phe per subunit	No. Tyr per subunit	No. Trp per subunit	Subunit pI[d]	Subunit charge at pH studied[d]
Azurin (α-helix and β-sheet)	4	128	13.9	6	2	1	5.7	−2.8
bG-CSF (α-helix)	1	174	18.9	6	3	1	6.6	−0.8[e] +17.1[f]
HSA (α-helix)	2	584	66.2	31	18	1	5.6	−15.0
KGF-2 (β-sheet)	1	140	16.2	6	9	2	9.9	+16.7
L-Asp.[g] (α-helix)	4	326	34.6	8	12	1	5.6	−11
Melittin (random)	NS	26	2.85	0	0	1	12.4	+5.0
RNase T1 (random)	1	130	14.0	4	10	1	4.1	−8.9

[a] Sequence information obtained from either the supplier or the CAS registry.
[b] As determined by CD spectroscopy; circular dichroism spectra are shown in the Supplemental Material.
[c] Number of subunits determined from PDB structures with ≥90% sequence homology with the proteins analyzed spectroscopically. The following PDB IDs were used: 4AZU (azurin) (Nar et al. 1991); 1BGC (bG-CSF) (Lovejoy et al. 1993); 1AO6 (HSA) (Sugio et al. 1999); 1I0V (RNase T1) (De Swarte et al. 2001). No crystal structures (NS) were available for KGF-2 or melittin.
[d] Calculated at http://www.embl-heidelberg.de/cgi/pi-wrapper.pl using the sequence information, if not provided by the supplier.
[e] pH 7.0.
[f] pH 3.0.
[g] L-Asparaginase (L-Asp.); sequence information obtained from the Protein Data Bank (http://www.rcsb.org/pdb/) (Berman et al. 2000), PDB ID 3ECA (Swain et al. 1993).

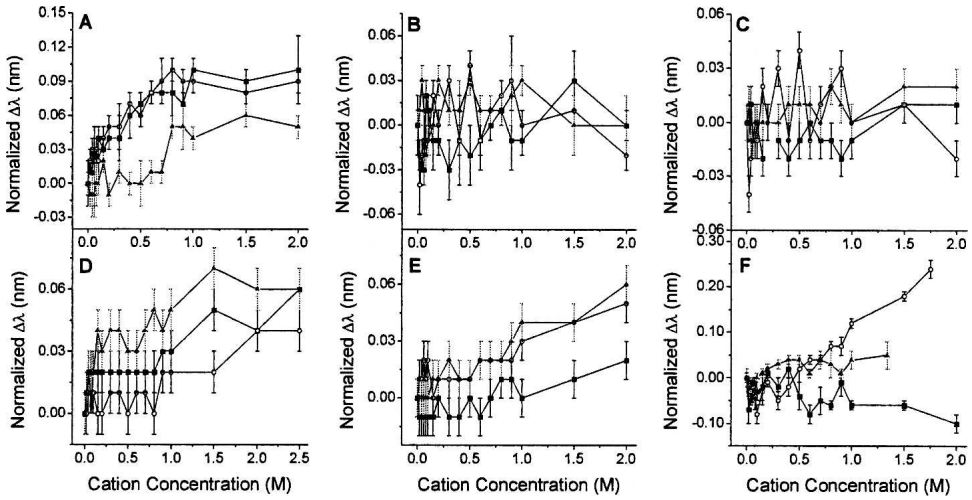

Figure 2. Phe peak shifts in the second-derivative UV absorption spectra of several proteins, KGF-2 (*A*), RNase T1 (*B*), bG-CSF (*C*), azurin (*D*), HSA (*E*), and L-asparaginase (*F*), induced by the cations Li^+ (■), Na^+ (○), and Cs^+ (▲). The data are displayed as in Figure 1, with initial peak positions of 258.93 ± 0.01 nm (*A*), 259.42 ± 0.02 nm (*B*), 259.04 ± 0.01 nm (*C*), 259.54 ± 0.01 nm (*D*), 259.31 ± 0.01 nm (*E*), and 259.68 ± 0.04 nm (*F*). Error bars represent the standard deviation of the mean for $n = 3$ for each salt.

due to the additive effects of cation–π interactions with multiple Phe residues. The Phe peak shift data for L-asparaginase (Fig. 2F) illustrates, however, that pronounced shifts may still be observed even if the solvent accessibility is relatively low. This observation suggests the importance of electrostatic components of cation–π interactions, which may help drive penetration of cations into less exposed regions of the protein. Conversely, bG-CSF and HSA, which have Phe residues with greater solvent accessibility compared to the other proteins, show less dramatic shifts. Thus, other factors must be affecting the magnitudes of these shifts (see Discussion below).

Figure 3 shows the shift in UV peak position near 290 nm as a function of salt concentration for the Trp residues of several proteins. The direction of Trp peak shifts is usually highly sensitive to the microenvironment of each residue, with blue shifts in UV spectra and red shifts in fluorescence spectra generally indicating increased solvent exposure (Rexroad et al. 2003). Melittin is a small, positively charged polypeptide under neutral pH conditions (Table 2) and contains no Phe or Tyr residues. Salts induce a red shift in the melittin Trp peak similar to that seen with *N*-acetyl-L-tryptophan ethyl (cf. Fig. 3A with 1B). Sodium ions induce the largest shift, followed by Li^+ and Cs^+, a trend that is similar to that seen with the model Trp compound. The magnitudes of the peptide's peak shifts, however, are much larger than those observed in the amino acid. It is clear in this case that the positively charged side chains of melittin do not significantly inhibit the ability of the cations to interact with the Trp indole ring. Increased ionic strength causes tetramerization of melittin (Faucon et al. 1979; Talbot et al. 1979) and also induces a secondary structure change as observed by circular dichroism (CD) (Supplemental Fig. S19). Fluorescence spectra reveal that high concentrations of all three cations cause major blue shifts in the emission maximum of Trp (Supplemental Table S1), a result indicating that the Trp residues have become shielded from solvent due to tetramerization or other structural changes. Increasing concentrations of Cs^+ resulted in quenched fluorescence (Supplemental Fig. S22), consistent with the findings of Lakowicz et al. (1983) and suggest that although the Trp residues are solvent shielded, they are still accessible to cations. Several of the proteins failed to show significant quenching of their fluorescence when titrated with Cs^+ ion but did show shifts in the second-derivative UV absorption peak position. This observation suggests the possibility of cation–π interaction without significant collisional quenching by the Cs^+ ion. This may reflect the fact that Cs^+ is often not an effective quencher of indole in contrast to its effectiveness with tyrosine side chains. The second-derivative UV absorption spectra exhibit an opposite, yet consistent trend relative to the fluorescence data, with the red shifts shown in Figure 3A indicating that the Trp residues have become more solvent shielded, while the large magnitude of the shifts suggest that the four Trp residues are still highly accessible to cations.

Azurin (Fig. 3E) and RNase T1 (Fig. 3C) both exhibit red shifts for all three salts like that seen for the model amino acid and melittin, but the shift magnitudes are much smaller. These results suggest that the Trp residues are relatively buried, which is corroborated by the solvent accessible surface calculations (Table 3) and fluorescence peak positions indicating that the Trp environment in both proteins is solvent shielded (319.5 ± 0.7 nm, azurin;

Table 3. *Solvent accessible surface areas (A^2) of aromatic amino acids determined by analysis of protein crystal structures*

Protein	No. residues	Total area	Mean	Median	Low	High
Phe						
Azurin	24	14.21	2.37	0.92	0.00	7.34
bG-CSF	6	302.47	50.41	62.15	3.67	84.13
HSA	62	895.60	28.89	25.33	0.00	77.88
L-Asp.	32	88.26	11.03	4.88	0.08	43.28
RNaseT1	4	87.69	21.92	21.69	0.00	44.30
Trp[a]						
Azurin	4	0.00	0.00	NA	NA	NA
bG-CSF	1	70.39	70.39	NA	NA	NA
HSA	2	84.42	84.42	NA	NA	NA
L-Asp.	4	0.13	0.13	NA	NA	NA
RNaseT1	1	7.50	7.50	NA	NA	NA
Tyr						
Azurin	8	17.77	8.88	8.88	4.48	13.28
bG-CSF	3	127.96	42.65	38.83	6.23	82.89
HSA	36	686.64	38.15	37.35	5.08	68.38
L-Asp.	48	255.77	21.31	21.77	0.00	56.28
RNaseT1	9	151.64	16.85	17.17	0.00	40.49

Protein crystal structures obtained from the Protein Data Bank (www.rcsb.org/pdb) (Berman et al. 2000). PDB IDs are as follows: 4AZU (azurin; tetramer) (Nar et al. 1991); 1BGC (bG-CSF; monomer) (Lovejoy et al. 1993); 1AO6 (HSA; dimer) (Sugio et al. 1999); 3ECA (L-asparaginase, L-Asp.; tetramer) (Swain et al. 1993); 1I0V (RNase T1; monomer) (De Swarte et al. 2001). Solvent-accessible surface areas for each residue were tabulated as a total value for all subunits. Average values for each residue were then calculated by dividing by the number of subunits. Reported total areas represent the sum of the average values for each residue, while the reported mean represents the overall average for all residues of each type in the protein.

[a]Proteins listed contain only one Trp per subunit; therefore, the median, low, and high values are not applicable.

323.5 ± 1.0 nm, RNase T1). RNase T1 showed increased fluorescence intensity at high salt concentrations. Only a high concentration of Li^+ (2.0 M), a known chaotropic agent, appeared to decrease the amount of secondary structure in RNase T1 (Supplemental Fig. S19); otherwise both proteins were conformationally stable at the salt concentrations used. Although no significant cation–π interactions between Trp and Lys or Arg were found by CaPTURE analysis, Cs^+ quenching was not observed in the fluorescence spectra (data not shown). The lack of Cs^+ quenching observed for RNase T1 may suggest a subtle change in tertiary structure at high salt concentrations that would not be detected by CD, which primarily measures protein secondary structure. Azurin, containing Cu^{2+}, exhibited relatively weak fluorescence in the absence of Li^+, Na^+, or Cs^+. Thus, quenching was not necessarily expected.

Quite different behavior is seen for the KGF-2 290-nm Trp peak (Fig. 3B), although both proteins are positively charged near neutral pH (Table 2). Results from CD and intrinsic fluorescence experiments (Supplemental Fig. S18 and Table S1) performed under solution conditions identical to that of the UV absorption measurements indicate that increasing the salt concentrations does not significantly alter KGF-2 secondary or tertiary structure, respectively, despite it belonging to a class of very conformationally sensitive proteins (Mach and Middaugh 1995; Edwards et al. 2001). Fluorescence quenching induced by Cs^+ is observed (Supplemental Fig. S22), indicating that the Trp residues are accessible. The salts induce a blue shift in Trp peak position in the second-derivative UV spectra rather than the red shift observed in melittin and in the isolated amino acid. Blue shifts in Trp peak position in UV absorption spectra are generally indicative of increased solvent exposure of these residues. Interestingly, the fluorescence emission maximum of KGF-2, although confirming that the residues are at least partially solvent exposed, remains relatively constant across the salt concentrations employed (341.6 ± 1.3 nm over 0.01–2.0 M salt concentrations, Supplemental Table S1). This suggests that this shift cannot be accounted for by changes in solvent polarity alone, and that additional mechanisms may be involved, as has been suggested previously for similar shifts observed in the Tyr peak positions. KGF-2 contains fewer Trp residues than oligomerized melittin, possibly contributing to the lower magnitude of the shifts (80% less).

L-Asparaginase (Fig. 3G) is similar to the tetrameric form of melittin in that it contains four Trp residues; however, the peak shift data is relatively noisy for this protein, with no clear trends apparent. CD spectra indicate no major effect of high salt concentrations on the secondary structure of this protein (Supplemental Fig. S20). The solvent accessible surface calculation in Table 3 and the fluorescence emission maximum (322.8 ± 0.2 nm over 0.01–2.0 M salt concentrations, Supplemental Table S1) indicates that the Trp residues are highly buried (i.e., solvent shielded), explaining why the cations do not penetrate effectively into the apolar interior of this protein. The large size and negative surface charge of L-asparaginase may also inhibit cation diffusion. No Cs^+ quenching of Trp fluorescence was observed for L-asparaginase, and the emission intensity for all three cations was relatively weak (a factor of 10 less than the data shown in Supplemental Fig. S22), also suggesting restricted cation diffusion into the protein's interior. Furthermore, CaPTURE analysis reveals that all four Trp residues are involved in energetically significant cation–π interactions with nearby Arg residues (Gallivan and Dougherty 1999; J.P. Gallivan, I. See, D. Elmore, and D.A Dougherty, http://capture.caltech.edu/). Similarly, the Trp residues of HSA, although more solvent exposed (Table 3), are involved in cation–π interactions with Lys residues. Thus no Cs^+ quenching of fluorescence was observed. In fact, a well-resolved Trp peak was not even observed in the second-derivative UV spectra of HSA. The results shown in Figure 3F are for the

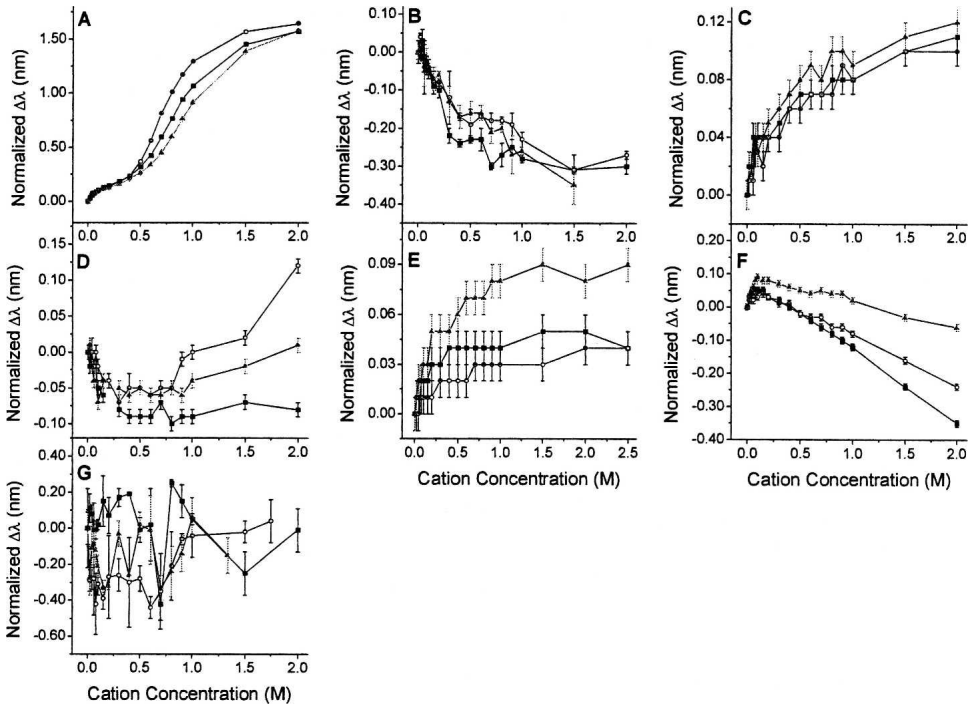

Figure 3. Trp peak shifts in the second-derivative UV absorption spectra of several proteins, melittin (*A*), KGF-2 (*B*), RNase T1 (*C*), bG-CSF (*D*), azurin (*E*), HSA (*F*), and L-asparaginase (*G*), induced by the cations Li^+ (■), Na^+ (○), and Cs^+ (▲). The data are displayed as in Figure 1, with initial peak positions of 290.02 ± 0.01 nm (*A*), 290.83 ± 0.02 nm (*B*), 291.99 ± 0.01 nm (*C*), 290.78 ± 0.01 nm (*D*), 292.53 ± 0.01 nm (*E*), and 286.75 ± 0.01 nm (*F*, Tyr/Trp), and 298.74 ± 0.09 nm (*G*). Error bars represent the standard deviation of the mean for $n = 3$ for each salt.

Tyr/Trp mixed peak at 287 nm and should therefore be interpreted cautiously.

The Trp peak of bG-CSF (Fig. 3D) manifests changes implying protein structural changes. These results are not surprising, given the extreme lability of this protein (Kueltzo and Middaugh 2003; Kueltzo et al. 2003). The Trp residue has a relatively high degree of solvent accessibility in the absence of salt (Table 3). The salts cause an initial blue shift in the Trp peak position, followed by a marked red shift beginning at 0.5–0.7 M salt concentration. The reversal of the trend in peak position suggests that the protein structure is altered by higher salt concentrations. Protein aggregation was simultaneously monitored by optical density values at 350 nm as a function of salt concentration. The optical density increased noticeably near 0.5 M salt, and visible aggregates were observed. Sodium ion caused the largest increase in optical density as well as the greatest red shift in the second-derivative UV spectra. The fluorescence emission peak position of Trp in bG-CSF suggested a more exposed Trp residue (λ_{max} = 343.6 nm in the absence of salt). This maximum remained essentially constant at low and intermediate salt concentrations but shifted to lower wavelength by 1–2 nm at high salt concentration (2.0 M), suggesting that the Trp had become more buried. Increasing salt concentrations also decreased the amount of α-helix as observed by CD but induced no other secondary structure change.

The Tyr peak shift data for the six proteins are presented in Figure 4. These peak shifts may reveal additional information about protein structure and dynamics, especially since the electronic state of this amino acid is influenced by ionic strength and the direction of the shifts can indicate hydrogen bond formation. Although multiple UV absorbance peaks are observed for tyrosine, the data shown in Figure 4 represent the pure tyrosine peak at 277 nm, which does not overlap any of the tryptophan signals. The peak shifts for RNase T1 (Fig. 4B) are similar to those observed for the free amino acid analog (Fig. 1C). Increasing the cesium ion concentration causes a red shift in the Tyr peak position, while Na^+ causes an intermediate change and Li^+ a blue shift. Although the peak shifts are small, the similarity of these data to that of *N*-acetyl-L-tyrosine ethyl ester suggests, not unexpectedly, that one or more of the protein's Tyr residues are located near the surface. The average solvent-accessible surface area for the Tyr residues of RNase T1 is relatively low (Table 3), but the range of areas reveals that indeed some of the Tyr residues are near the protein's surface. In contrast to Trp, the environment of Tyr cannot be further assessed from peak position in fluorescence spectra.

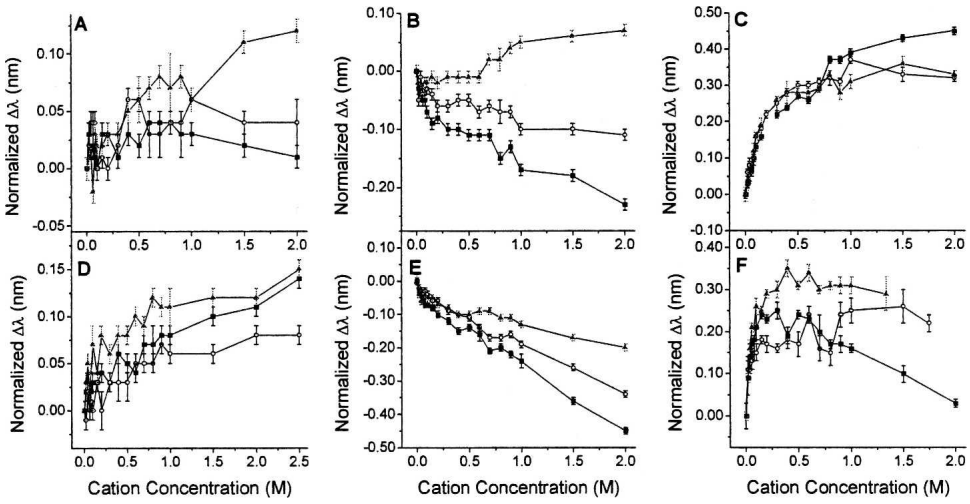

Figure 4. Tyr peak shifts in the second-derivative UV absorption spectra of several proteins, KGF-2 (*A*), RNase T1 (*B*), bG-CSF (*C*), azurin (*D*), HSA (*E*), and L-asparaginase (*F*), induced by the cations Li^+ (■), Na^+ (○), and Cs^+ (▲). The data are displayed as in Figure 1, with initial peak positions of 277.60 ± 0.01 nm (*A*), 277.61 ± 0.01 nm (*B*), 277.92 ± 0.01 nm (*C*), 274.86 ± 0.01 nm (*D*), 278.82 ± 0.01 nm (*E*), and 277.49 ± 0.01 nm (*F*). Error bars represent the standard deviation of the mean for $n = 3$ for each salt.

Trends in the second-derivative UV spectra contrary to the control data for free Tyr may indicate that the phenyl rings are buried, inaccessible, or that the protein structure has been perturbed. Small positive shifts in the Tyr peak position are observed with all salts for KGF-2 and azurin (Fig. 4A and D, respectively). Red shifts observed for all cations suggest that the auxochromic effect is dominating the peak positions rather than phenolate hydrogen bonding, which would be expected to cause a blue shift. Blue shifts in the data for the control amino acid were attributed to hydrogen bonding with the solvent or hydrated cation; thus, the predominance of red shifts for the Tyr peak shifts in KGF-2 and azurin suggest that the Tyr residues are buried in apolar regions of the protein and are much less accessible to the solvent. In particular, the Tyr residues of azurin do not have a high degree of solvent accessibility (Table 3). At salt concentrations >1.0 M, the differences in peak shifts for the three cations become more apparent. For KGF-2, Cs^+ causes the largest shift, while Na^+ and Li^+ cause similar shifts in azurin. The reason for these differences is unknown, although the magnitude and direction of such shifts may result from some charge repulsion at the protein surface that inhibits interaction of the cations with surface tyrosines or restricted diffusion of the cations to more buried tyrosines.

All three salts induce a relatively large red shift in the bG-CSF Tyr peak (Fig. 4C). As was observed for KGF-2, red shifts induced by all three cations suggest that the Tyr residues are generally buried and not extensively solvent exposed. The average solvent accessible surface area of Tyr in bG-CSF in the absence of salt is relatively large compared to the other proteins analyzed (Table 3), but these calculations do not account for structural changes induced by high salt concentrations. The magnitudes of the red shifts observed for the bG-CSF Tyr peak are much greater than for KGF-2, and thus the Tyr residues appear to be more accessible to the cations under the solution conditions studied. At concentrations >0.5 M, where the protein noticeably aggregates, Li^+ causes a greater peak shift than Na^+ or Cs^+. This suggests that the smaller cation penetrates more effectively into apolar regions of the aggregated protein.

In contrast, the three cations induce a large blue shift in the HSA Tyr peak position (Fig. 4E). It appears that hydrogen bonding effects are dominating the observed peak shifts in the presence of all three cations. The Tyr residues of this protein have a relatively high degree of solvent exposure compared to Tyr residues in the other proteins studied (Table 3). The relatively large magnitude of the salt-induced peak shifts is consistent with a high degree of accessibility to cations. Although the auxochromic effect dominated the shift for the model amino acid in the presence of Cs^+, its effect may still be seen in the relatively smaller magnitude of the blue shift of HSA Tyr compared to the other cations. The largest shift is seen for Li^+, the largest unhydrated cation (Table 1), followed by Na^+ and Cs^+. The same trend is observed for the Tyr/Trp peak of HSA (Fig. 3F).

The second-derivative UV absorption peak shifts of the Tyr residues in L-asparaginase are interesting in that all three cations cause red shifts at all concentrations studied, but the trends for each cation as a function of concentration are different. Cesium ion causes a large red shift (~0.30 nm) at low concentration that appears to reach a plateau.

Sodium ion causes a somewhat similar shift, with the initial plateau of 0.15 nm reached by 0.2 M salt, but a second red shift of 0.10 nm is seen beginning at 1.0 nm. Lithium ion, in contrast, causes an initial red shift that decreases as the salt concentration is increased. Due to the large number of Tyr residues in this protein (Table 2), there may be an array of microenvironments making interpretation of these results more difficult, even though the protein's secondary and tertiary structure was resilient to the presence of high salt concentrations (Supplemental Fig. S20). Indeed, the calculated solvent-accessible surface areas for the Tyr of this protein do cover a broad range (Table 3).

An additional application of this approach to immunoglobulins is contained in the Supplemental Material.

Effects of pH and temperature

Protein conformation is very sensitive to its immediate environment, with extremes in pH and temperature often inducing major structural alterations. Aromatic amino acid UV absorbance peak positions are also sensitive to the local environment of the side chains and can thus be sensitive to protein conformational changes (Donovan 1973; Solli and Herskovits 1973; Ichikawa and Terada 1979; Kueltzo et al. 2003). Although these changes are typically small compared to those detected by Trp fluorescence alterations, they are highly reproducible due to the diode array–based technology employed here (Kueltzo et al. 2003). In the unfolded state, buried amino acids generally become more solvent exposed and should therefore be more accessible to cations present in solution. Protein association, or aggregation, however, may result in more extensive burial of such residues. To demonstrate the detectability of such effects, bG-CSF was selected given the ability to modulate its conformational state by mild alterations of temperature and pH (Kueltzo and Middaugh 2003). Figure 5 shows the peak positions for selected Phe, Trp, and Tyr second-derivative absorbance bands of bG-CSF at low pH as a function of temperature. Compared to analogous data acquired at 10°C and pH 7 (Fig. 2C, Phe; Fig. 3D, Trp; and Fig. 4C, Tyr), the general trends in peak shifts are similar. All cations induce red shifts as their concentration is increased. Figure 5G shows the corresponding optical density monitored at 350 nm. This indicates that slight aggregation begins at ~0.6 M salt at 10°C and becomes

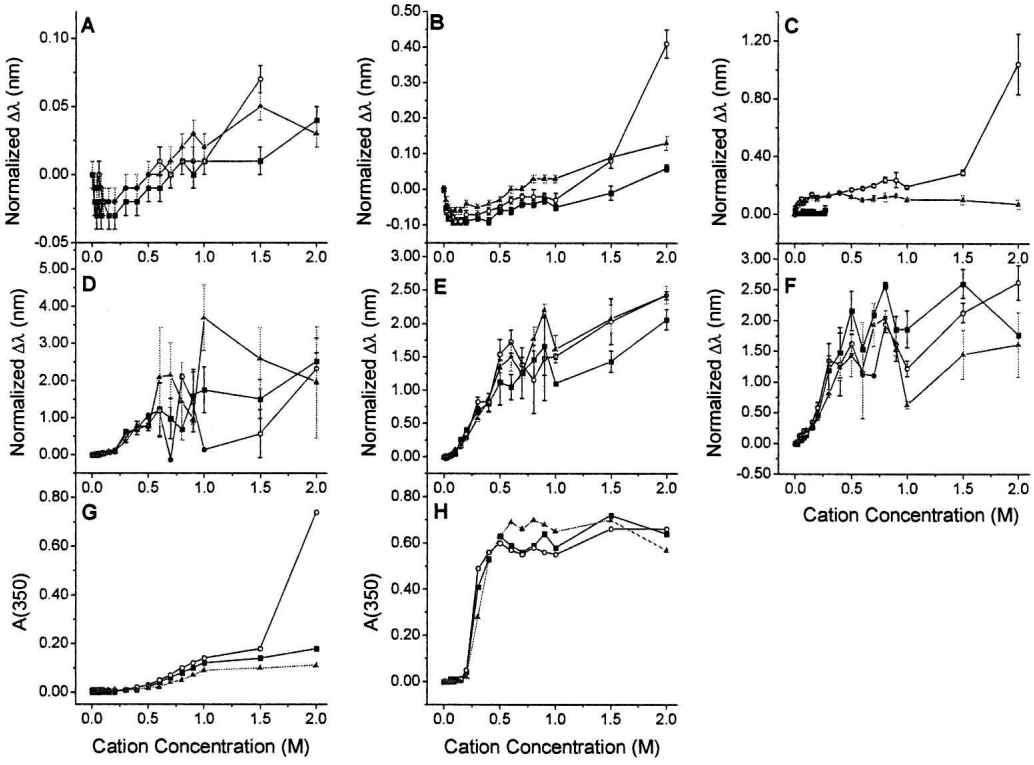

Figure 5. Peak shifts in the second-derivative UV absorption spectra of bG-CSF at pH 3.0 and 10°C (*A–C*) or 50°C (*D–F*) induced by the cations Li^+ (■), Na^+ (○), and Cs^+ (▲). The data are displayed as in Figure 1, with initial peak positions of 259.05 ± 0.01 nm (*A*, Phe), 290.86 ± 0.01 nm (*B*, Trp), 277.70 ± 0.01 nm (*C*, Tyr), 259.25 ± 0.01 nm (*D*, Phe), 290.83 ± 0.01 nm (*E*, Trp), and 277.61 ± 0.01 nm (*F*, Tyr). Error bars represent the standard deviation of the mean for $n = 3$ for each salt. Aggregation traces were monitored by optical density measurements (absorbance plus light scattering) at 350 nm for data acquired at 10°C (*G*) and 50°C (*H*).

more pronounced at concentrations >1.0 M. Sodium ion causes the largest increase in optical density, and this is directly mirrored in the Trp and Tyr peak shifts (Fig. 5B and C, respectively). This is contrary to the predictions of Hofmeister series behavior that strongly hydrated cations would be expected to destabilize proteins in the order $Li^+ > Na^+ > Cs^+$ (Hofmeister 1888; Kunz et al. 2004).

As the temperature is increased to 50°C, bG-CSF is on the verge of a major structural transition (Kueltzo and Middaugh 2003; Kueltzo et al. 2003). This transition involves the formation of aggregates and a change in secondary structure from α-helix to more disordered forms (Kueltzo and Middaugh 2003; Kueltzo et al. 2003). Aggregation at higher temperature is clearly exacerbated with increased salt concentration (Fig. 5H). Although the protein self-associates, the transition from helix to disordered structure seems to increase the accessibility of the aromatic amino acids to cations, as shown by very large peak shifts in Figure 5D–F.

Additional examples are provided in Figure 6. Figure 6A–C can be compared with Figures 2E, 3F, and 4E to characterize the effects of temperature on the peak positions of the aromatic residues of HSA. No aggregation was detected for this protein, but at 50°C HSA begins to lose some of its α-helical structure (Wetzel et al. 1980; Moriyama and Takeda 2005; see also Supplemental Fig. S21). The magnitudes and directions of the peak shifts for Phe are very similar at low and elevated temperatures. The three cations induce blue shifts in the Tyr/Trp peak at both temperatures, but the magnitudes of the shifts are less at higher temperature. The Tyr peak shifts at elevated temperature (Fig. 6F) are very noisy, in contrast to the distinct blue shifts seen at low temperature indicating significant hydrogen bonding and a high likelihood of solvent exposure. Thus, as HSA begins to undergo a structural change, the hydrogen bonding of Tyr is disrupted and these residues presumably become more buried in apolar regions of the protein.

Figure 6D–F illustrate the second-derivative UV peak positions for KGF-2 at 30°C, a temperature at which the protein has been observed to undergo conversion to a molten-globule-like state (Derrick et al. 2006). Figures 2A, 3B, and 4A show the corresponding data for the protein at 10°C. Aggregation in this case is much less than that seen

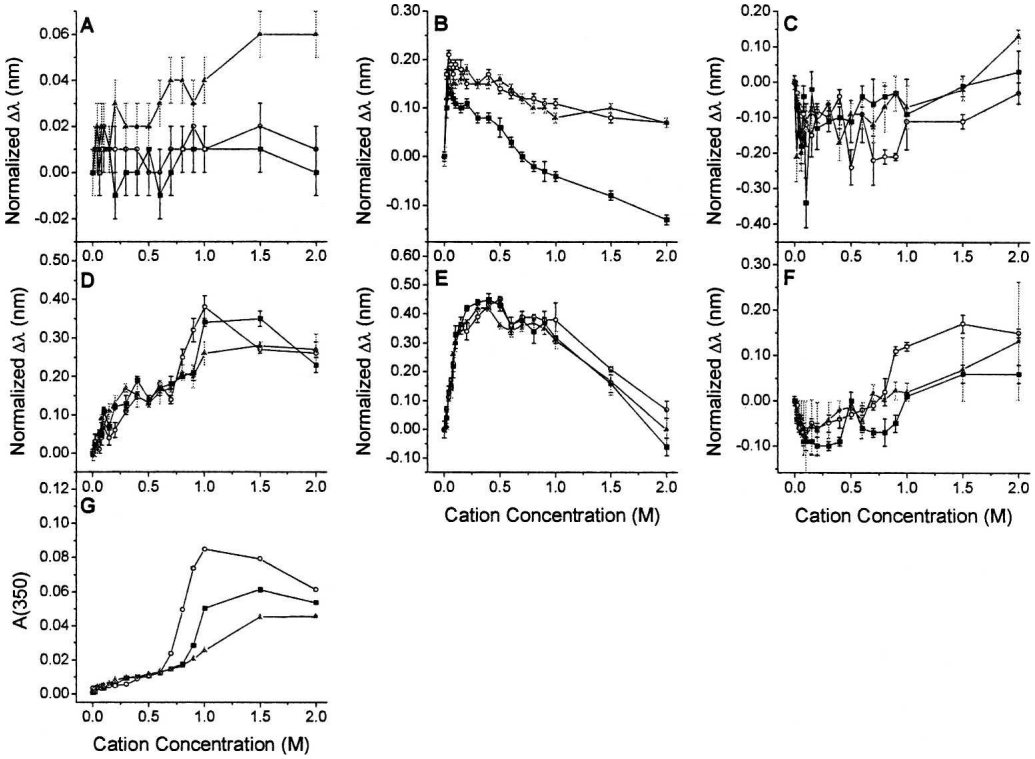

Figure 6. Peak shifts in the second-derivative UV absorption spectra of HSA at pH 7.0 and 50°C (*A–C*) or KGF-2 at pH 6.2 and 30°C (*D–F*) induced by the cations Li^+ (■), Na^+ (○), and Cs^+ (▲). The data are displayed as in Figure 1, with initial peak positions of 259.62 ± 0.01 nm (*A*, Phe), 286.30 ± 0.03 nm (*B*, Tyr/Trp), 278.63 ± 0.02 nm (*C*, Tyr), 259.05 ± 0.01 nm (*D*, Phe), 291.00 ± 0.01 nm (*E*, Trp), and 277.54 ± 0.01 nm (*F*, Tyr). Error bars represent the standard deviation of the mean for $n = 3$ for each salt. Aggregation traces were monitored by optical density measurements (absorbance plus light scattering) at 350 nm for the KGF-2 data acquired at 30°C (*G*).

for bG-CSF, although clearly present (Fig. 6G). The extent of aggregation, however, appears significantly different for the three cations at concentrations >0.6 M, with Na^+ again inducing a higher optical density at 350 nm and therefore the greater amount of aggregation. A major difference in the trends in the data for the two temperatures is observed for the Trp peak. At low temperature (Fig. 3B), the salts induce a blue shift in the 290-nm peak. At higher temperature (Fig. 6B), the salts initially produce a red shift followed by a blue shift. The blue shift begins to occur between 0.5 and 0.6 M salt, consistent with the increase in optical density indicating aggregation (Fig. 6G). The initial red shift in the second-derivative UV spectra suggests that the Trp residues are buried; however, the intrinsic fluorescence peak positions indicate that the residues are relatively solvent exposed (λ_{max} = 342.6–345.0 nm for all salts; see Supplemental Table S1). These conflicting results may reflect the presence of the molten globule state seen at high salt concentrations.

Discussion

Limitations of a simple diffusion model

The original basis of this work was the simple hypothesis that smaller cations would be able to diffuse into protein interiors more easily to interact with apolar aromatic residues. Thus, by analogy to solute fluorescence quenching methods, we imagined that dynamic aspects of a protein's polypeptide matrix should control the process. Therefore, we initially anticipated that the smallest unhydrated cation, lithium, would cause the greatest shifts in the UV absorbance spectra, followed by sodium and then cesium ion. Tables 4–6 summarize the UV absorbance peak shifts produced by Li^+, Na^+, and Cs^+ and are useful in conjunction with the data presented in Figures 2–6 for evaluating the hypothesis.

Table 4 shows the average Tyr peak shifts as a function of cation concentration in the second-derivative UV spectra. High salt concentrations were used in an attempt to drive the diffusion of cations into apolar regions of the proteins and thus facilitate cation–π interactions. Azurin, which contains several solvent-shielded Tyr residues (Table 3), exhibits very small peak shifts that are approximately equal for all three cations at high concentrations. RNase T1 and L-asparaginase contain some buried and some more exposed Tyr residues. Lithium ions cause the largest blue shift in RNase T1, followed by Na^+, and the largest unhydrated cation, Cs^+, actually causes a red shift, presumably due to the auxochromic effect. All Tyr peak shifts for L-asparaginase are to longer wavelengths and parallel the unhydrated cation radii: Li^+ produces the smallest shift, Na^+ an intermediate shift, and Cs^+ the largest shift. The data for KGF-2 at both temperatures studied exhibit a similar trend, although no crystal structure was available to calculate solvent-accessible surface areas of this protein's Tyr residues.

bG-CSF and HSA contain Tyr residues that are generally more solvent exposed than in the other proteins. The second-derivative UV peaks for these residues shifted to either shorter (bG-CSF) or longer (HSA) wavelengths, depending on the dominance of auxochromic or H-bonding effects, respectively, but Cs^+ caused the smallest shift. For HSA, whose secondary and tertiary structure was not seriously perturbed as a function of salt concentration or temperature, the smallest unhydrated cation, Li^+ caused the largest shift. Sodium ions caused the largest red shifts in the Tyr peaks of bG-CSF at low pH but also caused the greatest extent of aggregation (Fig. 5G,H).

Table 4. *Average tyrosine (~277 nm) peak shifts as a function of cation concentration*

Protein	Concentration	Li^+	Na^+	Cs^+
Azurin	0.1 M	0.03 (0.01)	0.00 (0.01)	0.07 (0.02)
10°C	0.5 M	0.05 (0.01)	0.03 (0.02)	0.08 (0.01)
pH 7.0	2.0 M	0.11 (0.01)	0.08 (0.01)	0.12 (0.01)
bG-CSF	0.1 M	0.13 (0.01)	0.16 (0.01)	0.16 (0.02)
10°C	0.5 M	0.27 (0.01)	0.30 (0.01)	0.27 (0.02)
pH 7.0	2.0 M	0.45 (0.01)	0.32 (0.01)	0.33 (0.01)
bG-CSF	0.1 M	0.07 (0.02)	0.10 (0.01)	0.10 (0.02)
10°C	0.5 M	0.12 (0.02)	0.17 (0.02)	0.12 (0.01)
pH 3.0	2.0 M	0.27 (0.03)	1.04 (0.21)	0.07 (0.03)
bG-CSF	0.1 M	0.15 (0.05)	0.16 (0.02)	0.21 (0.03)
50°C	0.5 M	2.16 (0.32)	1.63 (0.16)	1.43 (0.34)
pH 3.0	2.0 M	1.77 (0.03)	2.62 (0.28)	1.61 (0.53)
HSA	0.1 M	−0.07 (0.01)	0.04 (0.01)	−0.05 (0.01)
10°C	0.5 M	−0.14 (0.01)	−0.11 (0.01)	−0.10 (0.01)
pH 7.0	2.0 M	−0.45 (0.01)	−0.34 (0.01)	−0.20 (0.01)
HSA	0.1 M	0.03 (0.02)	0.04 (0.01)	0.12 (0.01)
50°C	0.5 M	−0.03 (0.03)	0.06 (0.01)	0.08 (0.02)
pH 7.0	2.0 M	−0.16 (0.01)	−0.07 (0.02)	−0.04 (0.01)
KGF-2	0.1 M	0.00 (0.01)	0.00 (0.01)	0.02 (0.01)
10°C	0.5 M	0.02 (0.01)	0.06 (0.01)	0.06 (0.02)
pH 6.2	2.0 M	0.01 (0.01)	0.04 (0.01)	0.12 (0.01)
KGF-2	0.1 M	−0.09 (0.02)	−0.07 (0.01)	−0.08 (0.01)
30°C	0.5 M	0.00 (0.02)	−0.03 (0.01)	−0.01 (0.02)
pH 6.2	2.0 M	0.06 (0.02)	0.15 (0.01)	0.13 (0.01)
L-Asp.	0.1 M	0.21 (0.03)	0.15 (0.02)	0.26 (0.02)
10°C	0.5 M	0.24 (0.01)	0.17 (0.03)	0.31 (0.01)
pH 7.0	2.0 M	0.03 (0.01)	0.22 (0.02)	0.29 (0.04)[a]
RNase T1	0.1 M	−0.07 (0.01)	−0.03 (0.01)	−0.02 (0.01)
10°C	0.5 M	−0.11 (0.01)	−0.05 (0.01)	−0.01 (0.01)
pH 7.0	2.0 M	−0.23 (0.01)	−0.11 (0.01)	0.07 (0.01)

Peak shifts given with respect to peak position at 0 M salt. Initial peak positions are given in the appropriate figure legends. Errors (shown in parentheses) represent the standard deviation of the mean for $n = 3$.
[a]Peak position at 1.3 M CsCl for L-asparaginase (L-Asp.).

Table 5. *Average phenylalanine (~259 nm) peak shifts as a function of cation concentration*

Protein	Concentration	Li^+	Na^+	Cs^+
Azurin	0.1 M	0.02 (0.01)	0.01 (0.01)	0.02 (0.01)
10°C	0.5 M	0.02 (0.01)	0.00 (0.01)	0.03 (0.01)
pH 7.0	2.0 M	0.04 (0.01)	0.04 (0.01)	0.06 (0.01)
bG-CSF	0.1 M	0.00 (0.01)	−0.02 (0.01)	0.00 (0.01)
10°C	0.5 M	0.01 (0.01)	−0.02 (0.01)	0.01 (0.01)
pH 7.0	2.0 M	0.01 (0.01)	0.03 (0.01)	0.02 (0.01)
bG-CSF	0.1 M	−0.02 (0.01)	−0.02 (0.01)	−0.02 (0.01)
10°C	0.5 M	−0.01 (0.01)	0.00 (0.01)	0.00 (0.01)
pH 3.0	2.0 M	0.04 (0.01)	0.00 (0.01)	0.03 (0.01)
bG-CSF	0.1 M	0.03 (0.01)	0.06 (0.01)	0.04 (0.01)
50°C	0.5 M	0.80 (0.16)	1.06 (0.64)	0.75 (0.07)
pH 3.0	2.0 M	2.53 (0.62)	2.33 (0.43)	1.96 (1.50)
HSA	0.1 M	−0.01 (0.01)	0.02 (0.01)	0.00 (0.01)
10°C	0.5 M	0.00 (0.01)	0.01 (0.01)	0.01 (0.01)
pH 7.0	2.0 M	0.02 (0.01)	0.05 (0.01)	0.06 (0.01)
HSA	0.1 M	0.01 (0.01)	0.02 (0.01)	0.02 (0.01)
50°C	0.5 M	0.01 (0.01)	0.00 (0.01)	0.02 (0.01)
pH 7.0	2.0 M	0.00 (0.01)	0.01 (0.01)	0.06 (0.01)
KGF-2	0.1 M	0.04 (0.01	0.02 (0.01)	0.00 (0.01)
10°C	0.5 M	0.07 (0.01)	0.06 (0.01)	0.00 (0.02)
pH 6.2	2.0 M	0.10 (0.03)	0.09 (0.01)	0.05 (0.01)
KGF-2	0.1 M	0.11 (0.01)	0.07 (0.02)	0.07 (0.02)
30°C	0.5 M	0.14 (0.01)	0.13 (0.01)	0.13 (0.01)
pH 6.2	2.0 M	0.23 (0.02)	0.26 (0.03)	0.27 (0.04)
L-Asp.	0.1 M	−0.02 (0.02)	−0.08 (0.02)	0.00 (0.01)
10°C	0.5 M	0.00 (0.02)	0.02 (0.03)	0.04 (0.01)
pH 7.0	2.0 M	−0.05 (0.01)	0.24 (0.02)	0.05 (0.03)[a]
RNase T1	0.1 M	0.01 (0.01)	−0.01 (0.01)	−0.01 (0.01)
10°C	0.5 M	−0.02 (0.02)	0.04 (0.01)	0.03 (0.01)
pH 7.0	2.0 M	0.00 (0.01)	−0.02 (0.01)	0.00 (0.02)

Peak shifts given with respect to peak position at 0 M salt. Initial peak positions are given in the appropriate figure legends. Errors (shown in parentheses) represent the standard deviation of the mean for $n = 3$.
[a] Peak position at 1.3 M CsCl for L-asparaginase (L-Asp.).

Table 5 shows that the cation-induced peak shifts for Phe are generally very small (~0.01 nm) and in some cases noisy (Fig. 2). As mentioned previously, this is probably due in part to the relatively low extinction coefficient for this amino acid compared to Trp and Tyr. Minimal shifts in native proteins suggest that Phe residues remain buried in the apolar interior of the protein and that the core of the native structure is maintained in the presence of the cations, although CD and fluorescence spectroscopy should be used to confirm the secondary and tertiary structure, respectively, of proteins under such conditions. Much larger peak shifts are observed for KGF-2 and bG-CSF at elevated temperatures, probably due to high intrinsic solvent accessibility or major structural changes that increase the solvent accessibility of these residues. Conversely, smaller peak shifts were observed for HSA at elevated temperature, where secondary structure had begun to decrease but no major structural changes appeared to occur.

Surprisingly, Cs^+ causes the greatest peak shift for the Trp residues of azurin (Table 6), which are not solvent exposed (Table 3). Cesium is the largest unhydrated cation but the smallest hydrated cation (Table 1). Thus, some penetration of solvated cations would cause this trend. Sodium ions cause a noticeably larger shift in the Trp peak of bG-CSF, but this is probably related to structural changes induced by high salt concentrations (Fig. 6). Otherwise, there is relatively little distinction in the peak positions of the Trp residues in the other proteins with respect to cation size (Table 6). Intrinsic Trp fluorescence in proteins and peptides with exposed Trp residues (e.g., melittin, IgG, KGF-2, and bG-CSF, having

Table 6. *Average tryptophan (~290 nm) peak shifts as a function of cation concentration*

Protein	Concentration	Li^+	Na^+	Cs^+
Azurin	0.1 M	0.02 (0.01)	0.01 (0.01)	0.03 (0.01)
10°C	0.5 M	0.04 (0.01)	0.02 (0.01)	0.06 (0.01)
pH 7.0	2.0 M	0.05 (0.01)	0.04 (0.01)	0.08 (0.01)
bG-CSF	0.1 M	−0.05 (0.01)	−0.02 (0.01)	−0.07 (0.01)
10°C	0.5 M	−0.09 (0.01)	−0.05 (0.01)	−0.05 (0.01)
pH 7.0	2.0 M	−0.08 (0.01)	0.12 (0.01)	0.01 (0.01)
bG-CSF	0.1 M	−0.09 (0.01)	−0.09 (0.01)	−0.06 (0.01)
10°C	0.5 M	−0.06 (0.01)	−0.05 (0.01)	−0.03 (0.01)
pH 3.0	2.0 M	0.06 (0.02)	0.41 (0.04)	0.13 (0.02)
bG-CSF	0.1 M	0.05 (0.03)	0.09 (0.01)	0.10 (0.01)
50°C	0.5 M	1.12 (0.34)	1.54 (0.22)	1.35 (0.09)
pH 3.0	2.0 M	2.06 (0.15)	2.42 (0.06)	2.43 (0.13)
KGF-2	0.1 M	−0.05 (0.02)	−0.04 (0.02)	−0.04 (0.01)
10°C	0.5 M	−0.23 (0.01)	−0.19 (0.04)	−0.16 (0.03)
pH 6.2	2.0 M	−0.30 (0.01)	−0.27 (0.05)	−0.35 (0.05)[a]
KGF-2	0.1 M	0.33 (0.03)	0.30 (0.02)	0.30 (0.03)
30°C	0.5 M	0.43 (0.02)	0.45 (0.01)	0.36 (0.01)
pH 6.2	2.0 M	−0.06 (0.03)	0.07 (0.03)	0.00 (0.07)
L-Asp.	0.1 M	0.02 (0.03)	−0.31 (0.06)	−0.21 (0.06)
10°C	0.5 M	−0.01 (0.07)	−0.28 (0.07)	0.02 (0.07)
pH 7.0	2.0 M	−0.01 (0.12)	−0.04 (0.12)	−0.15 (0.10)[b]
Melittin	0.1 M	0.10 (0.01)	0.09 (0.01)	0.09 (0.01)
10°C	0.5 M	0.32 (0.01)	0.36 (0.01)	0.26 (0.01)
pH 7.0	2.0 M	1.57 (0.01)	1.64 (0.01)	1.57 (0.01)
RNase T1	0.1 M	0.04 (0.01)	0.03 (0.01)	0.03 (0.01)
10°C	0.5 M	0.07 (0.01)	0.06 (0.01)	0.08 (0.01)
pH 7.0	2.0 M	0.11 (0.01)	0.10 (0.01)	0.12 (0.01)

Peak shifts given with respect to peak position at 0 M salt. Initial peak positions are given in the appropriate figure legends. Errors (shown in parentheses) represent the standard deviation of the mean for $n = 3$.
[a] Peak position at 1.5 CsCl for KGF-2 at 10°C.
[b] Peak position at 1.3 M CsCl for L-asparaginase (L-Asp.).

fluorescence emission maxima >340 nm) was quenched by increasing Cs^+ concentration (Supplemental Fig. S22). Although Cs^+ is a known fluorescence quencher (Fasano et al. 2003), there appears to be no analogous trend in the intensity of the second-derivative UV absorbance peaks (Table 6). Significant quenching was not observed for proteins with buried Trp residues (λ_{max} < 340 nm, i.e., azurin, HSA, IgG, L-asparaginase, and RNase T1.)

The lack of consistent trends in the magnitude of the shifts of Phe and Trp peak position with cation size indicates some limitation of the diffusion-based physical model upon which our initial hypothesis was based. Although the majority of the experiments were conducted at or near neutral pH, most of the proteins studied are charged under these conditions. Dispersed positive charge on a protein's surface could potentially create a barrier repulsive to cation penetration into protein interiors, while negative charge can potentially compete with the π electrons of the aromatic rings. Clearly, however, surface charge does not itself prevent detection of peak shifts, as evidenced by blue shifts in Trp peak positions for KGF-2, which is very highly positively charged, at least in localized regions of the protein's surface (Fig. 3B; Table 2). Furthermore, specific or nonspecific binding of cations to protein sites other than aromatic rings (e.g., amide dipoles) may also influence the magnitude and direction of the peak shifts. In particular, this phenomenon could complicate interpretation of trends in peak shifts with respect to cation size, especially if one cation binds preferentially to additional sites. Collectively, these factors complicate interpretation of the results in light of a simple diffusion model, although the Tyr peak shifts of some proteins exhibit behavior supporting the initial hypothesis. Thus, we can propose the use of this approach as a direct probe of protein structure and dynamics if a clear trend in peak shifts is seen with increasing cation size.

Conclusions

The results presented here clearly show that several factors related to the local environment of aromatic amino acids influence the magnitude and direction of peak shifts in UV spectra of proteins to which cations have been added. Solvent accessibility seems to be important but not necessary for observing shifts, irrespective of whether the residue is buried in an apolar region or located on a protein's surface. Small, but reproducible, peak shifts can be observed even for solvent shielded residues (e.g., in azurin), providing evidence that cations penetrate into interior regions of proteins, permitting interaction with aromatic side chains. In contrast, when we titrated the proteins of the study with larger organic cations (e.g., trimethyl amine, triethyl amine, etc.) no shifts were seen (data not shown). This suggests that the small size of the metal cations perhaps combined with some specific polar interactions with hydrophilic sites in protein interiors may at least partially be responsible for the shifts seen. Nevertheless, the magnitude of the peak shift seems to at least partially depend upon the number of residues involved in cation–π interactions and restrictions in the diffusional path, which in turn depends on local dynamic fluctuations of the protein matrix. An increase or decrease in the magnitude of the peak shift can also indicate protein structural changes or aggregation. The local environment of each residue, governed in part by hydrogen bonding, interactions with nearby residues, and perturbation of protein structures induced by the presence of high salt concentrations, impacts the direction of the peak shift. Because the second-derivative method deconvolutes spectra only according to amino acid type (i.e., Phe, Trp, Tyr), unique information about individual residues in proteins cannot be obtained unless the protein contains a single residue of a specific amino acid. Thus, the peak shifts reflect the contributions of amino acids in multiple environments accessible to the cations by multiple diffusional paths.

Second-derivative UV absorbance spectroscopy provides useful information regarding the features of protein structure influencing cation–π interactions. This method has the potential to yield a more complete picture of protein structure and behavior than, for example, fluorescence quenching measurements, because the spectra for Phe, Trp, and Tyr are acquired in a single, rapid measurement and are generally well resolved by derivitization of the spectrum. Unlike fluorescence studies of proteins, which rely entirely on Trp residues, all three aromatic side chains are accessible to this technique. The variety of environments in which these residues are present, however, makes it difficult to unambiguously evaluate the influence of classes of structural features on protein dynamics that might facilitate or diminish cation–π interactions with external probes. In light of this progress toward our initial goals of characterizing protein structure and dynamics by second-derivative UV analysis using cationic probes, additional, carefully designed studies with model polypeptides may provide further insight into the role of noncovalent side chain interactions such as ion pairing, hydrogen bonding, and existing cation–π interactions as well as protein secondary and tertiary structure on cation–π interactions between aromatic amino acids and external probes.

Materials and methods

Materials

Ribonuclease T1 purified from *Aspergillus oryzae* was obtained from Epicentre. bG-CSF was a gift from Bioprocess Research and Development Department at Pfizer, Inc. KGF-2 was obtained from Human Genome Sciences, Inc. The antibody (IgG) was supplied by MedImmune. *N*-acetyl-L-phenylalanine ethyl

ester, *N*-acetyl-L-tryptophan ethyl ester, *N*-acetyl-L-tyrosine ethyl ester, melittin, and all other proteins were obtained from Sigma. Azurin was purified from *Pseudomonas aeruginosa*. All other materials were obtained from Sigma and Fisher Scientific.

Sample preparation

KGF-2 was supplied in a high salt buffer (20 mM sodium acetate, 125 mM NaCl, and 1 mM EDTA). Therefore, the sample was initially diluted seven times with deionized water to decrease the initial salt concentration. The final pH was 6.2. bG-CSF was dialyzed into 1 mM citrate buffer (pH 3.0 or 7.0). The antibody was prepared in 25 mM histidine HCl with 1.6 mM glycine (pH 6.0). All other samples were dialyzed into a generic buffer of 1 mM MOPS (pH 7.0). Dialysis was performed exhaustively using Pierce Slide-A-Lyzer dialysis cassettes. Stock solutions of the salts LiCl, NaCl, and CsCl were prepared at 5 M in the appropriate buffer of the corresponding protein. The buffers for each protein were chosen based on literature and experimental information to provide increased stability during the experiments.

Absorbance measurements and data analysis

High resolution absorbance spectra were obtained at 10.0 ± 0.1°C (unless otherwise noted) using an Agilent 8453 UV-visible spectrophotometer equipped with a diode array detector and Peltier temperature controller (HP 89090A). All samples were analyzed in a 3-mL quartz cuvet with a 1-cm path length. Titration experiments were performed both with protein samples and *N*-acetyl-L-tryptophan ethyl ester (37 μM), *N*-acetyl-L-tyrosine ethyl ester (146 μM), and *N*-acetyl-L-phenylalanine ethyl ester (510 μM) solutions (in water). Protein experiments were performed by incrementally adding concentrated (5.0 M) LiCl, NaCl, and CsCl to the sample with the amino acid concentration kept essentially constant, with spectra measured 3 min after each addition. Amino acid samples were prepared individually for each salt concentration examined. All proteins were analyzed at concentrations corresponding to ~0.1 absorbance units at 280 nm. The temperature was allowed to equilibrate for 3 min prior to the acquisition of each spectrum. Spectra were analyzed over the wavelength range 200–400 nm and collected with an integration time of 25 sec. The optical density at 350 nm was used to monitor protein aggregation. No significant aggregation was observed for most samples (but see Results). Second-derivative spectra were calculated using a nine-point data filter and third-order Savitzky–Golay polynomial in Chemstation software (Agilent). A spline function was applied to the resulting spectra using 99 interpolated points between each raw data point. This approach permits a resolution of 0.01 nm to be obtained under optimal conditions (Mach et al. 1991). All second-derivative spectra were exported to Microcal Origin version 6.0 or higher to determine peak positions. Results are reported with error bars representing the standard deviation of the mean from three independent measurements. In the case error bars are not seen, they are enclosed within the plotted symbol.

Structural studies

CD and intrinsic fluorescence experiments were performed to measure the effects of salt concentrations on protein secondary and tertiary structure, respectively. CD experiments were conducted with a Jasco J-810 spectropolarimeter as described previously (Kueltzo and Middaugh 2003). Additional details of the CD experiments and the resulting spectra are provided in the Supplemental Material. Protein solutions with 0.0, 0.1, 0.5, and 2.0 M LiCl, NaCl, or CsCl were prepared at concentrations to give ~0.1 M absorbance units at 280 nm. Fluorescence spectra were acquired on a PTI QuantaMaster spectrophotometer equipped with a four-position thermostated sample holder. Cuvets with a 1-cm path length were used. An excitation wavelength of 295 nm was used and spectra of Trp emission were acquired from 305–400 nm in 1-nm increments. The integration time was 1 sec, and the excitation and emission slits were set at 4 nm. The fluorescence spectra were measured under the same pH and temperature conditions as the absorbance spectra, after a 3-min thermal equilibration time. The appropriate buffer or buffer plus salt background spectrum was subtracted from each spectrum containing protein. The fluorescence spectra were then smoothed with a seven-point data filter (second-order Savitzky–Golay polynomial). The y-intercept of the first derivative of each smoothed spectrum was measured to find the maximum of the Trp emission peak for each protein at each salt concentration studied.

Molecular modeling

Solvent-accessible surfaces were calculated in Sybyl 7.0 (Tripos, Inc.). Protein crystal structures were obtained from the Protein Data Bank (Berman et al. 2000) and confirmed to have ≥90% sequence homology with the proteins analyzed by UV-visible spectroscopy. Aromatic amino acids in individual subunits were selected, and fast Connolly surfaces were generated. Lipophilic surface potentials were then determined using the standard parameter set and the Crippen table of Ghose et al. (1998). Solvent-accessible surfaces were calculated for each residue either individually (protein monomers) or collectively (proteins with multiple subunits). An average area for each residue was calculated by dividing by the number of subunits. The values for individual residues were then averaged to calculate the mean accessible surface area for each residue type in each protein. CaPTURE analysis was performed online (J.P. Gallivan, I. See, D. Elmore, and D.A Dougherty, http://capture.caltech.edu/) using the algorithm of Gallivan and Dougherty (1999) to evaluate cation–π interactions between the positively charged amino acids Lys and Arg and the aromatic amino acids Phe, Trp, and Tyr.

Electronic supplemental material

Second-derivative UV absorption peak shift data for all aromatic amino acids in the model compounds and proteins, CD spectra, fluorescence peak shifts for the proteins studied as a function of salt concentration, and fluorescence spectra demonstrating the effect of Cs^+ quenching Trp fluorescence are available at http://www.proteinscience.org.

Acknowledgments

We thank Melissa Perkins and Tom Spitznagel (Human Genome Sciences), Susan Martin (Pfizer), and Chris Allan (MedImmune) for a constant supply of large quantities of highly purified proteins that were critical for the success of these studies. We also thank Dr. Gerry Lushington for helpful assistance with the analysis of protein solvent-accessible surface areas and Nazila Salamat-Miller and Fatma Y. Ersen, who assisted with some of

the protein structural studies. This work was supported by Human Genome Sciences, Pfizer, Inc., and MedImmune.

References

Adams, P.D., Loh, A.P., and Oswald, R.E. 2004. Backbone dynamics of an oncogenic mutant of Cdc42Hs shows increased flexibility at the nucleotide-binding site. *Biochemistry* **43:** 9968–9977.

Balestrieri, C., Colonna, G., Giovane, A., Irace, G., and Servillo, L. 1978. Second-derivative spectroscopy of proteins. *Eur. J. Biochem.* **90:** 433–440.

———. 1980. Second-derivative spectroscopy of proteins: Studies on tyrosyl residues. *Anal. Biochem.* **106:** 49–54.

Berman, H.M., Westbrook, J., Feng, Z., Gilliland, G., Bhat, T.N., Weissig, H., Shindyalov, I.N., and Bourne, P.E. 2000. The Protein Data Bank. *Nucleic Acids Res.* **28:** 235–242.

Bohórquez, H.J., Obregón, M., Cárdenas, C., Llanos, E., Suárez, C., Villaveces, J.L., and Patarroyo, M.E. 2003. Electronic energy and multipolar moments characterize amino acid side chains into chemically related groups. *J. Phys. Chem. A* **107:** 10090–10097.

Derrick, T., Grillo, A.O., Vitharana, S.N., Jones, L., Rexroad, J., Shah, A., Perkins, M., Spitznagel, T.M., and Middaugh, C.R. 2006. Effect of polyanions on the structure and stability of RepiferminTM (Keratinocyte Growth Factor-2). *J. Pharm. Sci.* (in press).

De Swarte, J., De Vos, S., Langhorst, U., Steyaert, J., and Loris, R. 2001. The contribution of metal ions to the conformational stability of ribonuclease T1: Crystal versus solution. *Eur. J. Biochem.* **268:** 3993–4000.

Donovan, J.W. 1969. Ultraviolet absorption. In *Physical principles and techniques of protein chemistry* (ed. S.J. Leach). Part A, pp. 101–170. Academic Press, New York.

———. 1973. Ultraviolet difference spectroscopy–new techniques and applications. *Methods Enzymol.* **27:** 497–525.

Dougherty, D.A. 1996. Cation–π interactions in chemistry and biology: A new view of benzene, Phe, Tyr, and Trp. *Science* **271:** 163–168.

Edsall, J.T. and McKenzie, H.A. 1978. Water and proteins. I. The significance and structure of water; its interaction with electrolytes and non-electrolytes. *Adv. Biophys.* **10:** 137–207.

Edwards, K.L.T., Kueltzo, L.A., Fisher, M.T., and Middaugh, C.R. 2001. Complex effects of molecular chaperones on the aggregation and refolding of fibroblast growth factor-1. *Arch. Biochem. Biophys.* **393:** 14–21.

Fasano, M., Orsale, M., Melino, S., Nicolai, E., Forlani, F., Rosato, N., Cicero, D., Pagani, S., and Paci, M. 2003. Surface changes and role of buried water molecules during the sulfane sulfur transfer in Rhodanese from *Azotobacter vinelandii*: A fluorescence quenching and nuclear magnetic relaxation dispersion spectroscopic study. *Biochemistry* **42:** 8550–8557.

Faucon, J.F., Dufourcq, J., and Lussan, C. 1979. The self-association of melittin and its binding to lipids. An intrinsic fluorescence polarization study. *FEBS Lett.* **102:** 187–190.

Gallivan, J.P. and Dougherty, D.A. 1999. Cation–π interactions in structural biology. *Proc. Natl. Acad. Sci.* **96:** 9459–9464.

Ghose, A.K., Viswanadhan, V.N., and Wendoloski, J.J. 1998. Prediction of hydrophobic (lipophilic) properties of small organic molecules using fragmental methods: An analysis of ALOGP and CLOGP methods. *J. Phys. Chem. A* **102:** 3762–3772.

Giese, A.T. and French, C.S. 1955. The analysis of overlapping spectral absorption bands by derivative spectrophotometry. *Appl. Spectrosc.* **9:** 78–96.

Grum, F., Paine, D., and Zoeller, L. 1972. Derivative absorption and emission spectrophotometry. *Appl. Opt.* **11:** 93–98.

Harris, D.C. 1995. *Quantitative chemical analysis*. W.H. Freeman and Company, New York.

Hofmeister, F. 1888. Zur lehre von der wirkung der salze. *Arch. Exp. Pathol. Pharmakol.* **24:** 247–260.

Ichikawa, T. and Terada, H. 1977. Second derivative spectrophotometry as an effective tool for examining phenylalanine residues in proteins. *Biochim. Biophys. Acta* **494:** 267–270.

———. 1979. Estimation of state and amount of phenylalanine residues in proteins by second derivative spectrophotometry. *Biochim. Biophys. Acta* **580:** 120–128.

Ito, M. 1960. Ultraviolet absorption study of the molecular association of phenols. *J. Mol. Spectrosc.* **4:** 125–143.

Keniry, M.A. and Carver, J.A. 2002. NMR spectroscopy of large proteins. *Ann. Rep. NMR Spectrosc.* **48:** 31–69.

Kielland, J. 1937. Individual activity coefficients of ions in aqueous solutions. *J. Am. Chem. Soc.* **59:** 1675–1678.

Kueltzo, L.A. and Middaugh, C.R. 2003. Structural characterization of bovine granulocyte colony stimulating factor: Effect of temperature and pH. *J. Pharm. Sci.* **92:** 1793–1804.

Kueltzo, L.A., Ersoy, B., Ralston, J.P., and Middaugh, C.R. 2003. Derivative absorbance spectroscopy and protein phase diagrams as tools for comprehensive protein characterization: A bGCSF case study. *J. Pharm. Sci.* **92:** 1805–1820.

Kunz, W., Henle, J., and Ninham, B.W. 2004. Zur lehre von der wirkung der salze' (About the science of the effect of salts): Franz Hofmeister's historical papers. *Curr. Opin. Coll. Interface Sci.* **9:** 19–37.

Lakowicz, J.R., Maliwal, B.P., Cherek, H., and Balter, A. 1983. Rotational freedom of tryptophan residues in proteins and peptides. *Biochemistry* **22:** 1741–1752.

Levine, R.L. and Federici, M.M. 1982. Quantitation of aromatic residues in proteins: Model compounds for second-derivative spectroscopy. *Biochemistry* **21:** 2600–2606.

Lovejoy, B., Cascio, D., and Eisenberg, D. 1993. Crystal structure of canine and bovine granulocyte-colony stimulating factor (G-CSF). *J. Mol. Biol.* **234:** 640–653.

Ma, J.C. and Dougherty, D.A. 1997. The cation–π interaction. *Chem. Rev.* **97:** 1303–1324.

Mach, H. and Middaugh, C.R. 1994. Simultaneous monitoring of the environment of tryptophan, tyrosine, and phenylalanine residues in proteins by near-ultraviolet second-derivative spectroscopy. *Anal. Biochem.* **222:** 323–331.

———. 1995. Interaction of partially structured states of acidic fibroblast growth factor with phospholipid membranes. *Biochemistry* **34:** 9913–9920.

Mach, H., Thomson, J.A., Middaugh, C.R., and Lewis, R.L. 1991. Examination of phenylalanine microenvironments in proteins by second-derivative absorption spectroscopy. *Arch. Biochem. Biophys.* **287:** 33–40.

Moriyama, Y. and Takeda, K. 2005. Protective effects of small amounts of bis(2-ethylhexyl)sulfosuccinate on the helical structures of human and bovine serum albumins in their thermal denaturations. *Langmuir* **21:** 5524–5528.

Nar, H., Messerschmidt, A., van de Kamp, M., and Canters, G.W. 1991. Crystal structure analysis of oxidized *Pseudomonas aeruginosa* azurin at pH 5.5 and pH 9.0. A pH-induced conformational transition involves a peptide bond flip. *J. Mol. Biol.* **218:** 427–447.

Padrós, E., Morros, A., Mañosa, J., and Duñach, M. 1982. The state of tyrosine and phenylalanine residues in proteins analyzed by fourth-derivative spectrophotometry. *Eur. J. Biochem.* **127:** 117–122.

Poluektov, O.G., Utschig, L.M., Dalosto, S., and Thurnauer, M.C. 2003. Probing local dynamics of photosynthetic bacterial reaction center with a cysteine specific spin label. *J. Phys. Chem. B* **107:** 6239–6244.

Rexroad, J., Wiethoff, C.M., Green, A.P., Kierstead, T.D., Scott, M.O., and Middaugh, C.R. 2003. Structural stability of adenovirus type 5. *J. Pharm. Sci.* **92:** 665–678.

Rogers, D.M. and Hirst, J.D. 2003. Ab initio study of aromatic side chains of amino acids in gas phase and solution. *J. Phys. Chem. A* **107:** 11191–11200.

Ruan, C. and Rodgers, M.T. 2004. Cation–π interactions: Structures and energetics of complexation of $Na^+$and K^+ with the aromatic amino acids, phenylalanine, tyrosine, and tryptophan. *J. Am. Chem. Soc.* **126:** 14600–14610.

Ruiz, J.L., Ferrer, J., Pire, C., Llorca, F.I., and Bonete, M.J. 2003. Denaturation studies by fluorescence and quenching of thermophilic protein NAD^+-glutamate dehydrogeanse from *Thermus thermophilus* HB8. *J. Protein Chem.* **22:** 295–301.

Ryzhov, V., Dunbar, R.C., Cerda, B., and Wesdemiotis, C. 2000. Cation–π effects in the complexation of Na^+ and K^+ with Phe, Tyr, and Trp in the gas phase. *J. Am. Soc. Mass Spectrom.* **11:** 1037–1046.

Shannon, R.D. 1976. Revised effective ionic radii and systematic studies of interatomic distances in halides and chalcogenides. *Acta Crystallogr. A* **32:** 751–767.

Skoog, D.A., Holler, F.J., and Nieman, T.A. 1998. *Principles of instrumental analysis.*. Harcourt Brace and Company, Chicago.

Solli, N.J. and Herskovits, T.T. 1973. Solvent perturbation studies and analysis of protein and model compound data in denaturing organic solvents. *Anal. Biochem.* **54:** 370–378.

Sugio, S., Kashima, A., Mochizuki, S., Noda, M., and Kobayashi, K. 1999. Crystal structure of human serum albumin at 2.5 Å resolution. *Protein Eng.* **12:** 439–446.

Swain, A.L., Jaskolski, M., Housset, D., Rao, J.K., and Wlodawer, A. 1993. Crystal structure of *Escherichia coli* L-asparaginase, an enzyme used in cancer therapy. *Proc. Natl. Acad. Sci.* **90:** 1474–1478.

Talbot, J.C., Dufourcq, J., de Bony, J., Faucon, J.F., and Lussan, C. 1979. Conformational change and self association of monomeric melittin. *FEBS Lett.* **102:** 191–193.

Wetzel, R., Becker, M., Behlke, J., Billwitz, J., Boehm, S., Ebert, B., Hamann, J., Krumbiegel, J., and Lassman, G. 1980. Temperature behavior of human serum albumin. *Eur. J. Biochem.* **104:** 469–478.

Woods, A.S. 2004. The mighty arginine, the stable quaternary amines, the powerful aromatics, and the aggressive phosphate: Their role in the noncovalent minuet. *J. Proteome Res.* **3:** 478–484.

Yan, X., Watson, J., Ho, P.S., and Deinzer, M.L. 2004. Mass spectrometric approaches using electrospray ionization charge states and hydrogen–deuterium exchange for determining protein structures and their conformational studies. *Mol. Cell. Proteomics* **3:** 10–23.

Yu, S., Mei, F.C., Le, J.C., and Cheng, X. 2004. Probing cAMP-dependent protein kinase holoenzyme complexes Iα and IIβ by FT-IR and chemical protein footprinting. *Biochemistry* **43:** 1908–1920.

Yuan, Z., Zhao, J., and Wang, Z.-X. 2003. Flexibility analysis of enzyme active sites by crystallographic temperature factors. *Protein Eng.* **16:** 109–114.

Zhang, Z. and Smith, D.L. 1993. Determination of amide hydrogen exchange by mass spectrometry: A new tool for protein structure elucidation. *Protein Sci.* **2:** 522–531.